GA–A27699

ION FAST IGNITION — ESTABLISHING A SCIENTIFIC BASIS FOR INERTIAL FUSION ENERGY

Final Report

by
R.B. STEPHENS, M.E. FOORD, M.S. WEI, F.N. BEG,
and D. SCHUMACHER

Work supported by
the U.S. Department of Energy
under DE-SC0001265

DISCLAIMER

This report was prepared as an account of work sponsored by an agency of the United States Government. Neither the United States Government nor any agency thereof, nor any of their employees, makes any warranty, express or implied, or assumes any legal liability or responsibility for the accuracy, completeness, or usefulness of any information, apparatus, product, or process disclosed, or represents that its use would not infringe privately owned rights. Reference herein to any specific commercial product, process, or service by trade name, trademark, manufacturer, or otherwise, does not necessarily constitute or imply its endorsement, recommendation, or favoring by the United States Government or any agency thereof. The views and opinions of authors expressed herein do not necessarily state or reflect those of the United States Government or any agency thereof.

NOVEMBER 2013

GENERAL ATOMICS

GA–A27699

ION FAST IGNITION — ESTABLISHING A SCIENTIFIC BASIS FOR INERTIAL FUSION ENERGY

Final Report

by
R.B. STEPHENS, M.E. FOORD,* M.S. WEI, F.N. BEG†,
and D. SCHUMACHER‡

*Lawrence Livermore National Laboratory, Livermore, California.
†University of California San Diego, La Jolla, California.
‡Ohio State University, Columbus, Ohio.

Work supported by
the U.S. Department of Energy
under DE-SC0001265

DISCLAIMER

This report was prepared as an account of work sponsored by an agency of the United States Government. Neither the United States Government nor any agency thereof, nor any of their employees, makes any warranty, express or implied, or assumes any legal liability or responsibility for the accuracy, completeness, or usefulness of any information, apparatus, product, or process disclosed, or represents that its use would not infringe privately owned rights. Reference herein to any specific commercial product, process, or service by trade name, trademark, manufacturer, or otherwise, does not necessarily constitute or imply its endorsement, recommendation, or favoring by the United States Government or any agency thereof. The views and opinions of authors expressed herein do not necessarily state or reflect those of the United States Government or any agency thereof.

GENERAL ATOMICS PROJECT 30337
NOVEMBER 2013

GENERAL ATOMICS

Table of Contents

1. Executive Summary

We report on the proton-Fast Ignition (FI) component of the ion-FI project. It was a joint effort with Lawrence Livermore National Laboratory (LLNL) and Los Alamos National Laboratory (LANL) and was structured with separate foci on proton- and heavier-ion-mediated ignition. LANL focused on the heavier Z ions. General Atomics (GA), LLNL, and our subcontractors University of California San Diego (UCSD) and The Ohio State University (OSU) focused on the proton FI aspect of the program. It is the generation and transport of this proton beam that was the focus of the proton-FI program and which is reported here.

Our work has addressed a major scientific uncertainty in Relativistic High Energy Density (RHED) physics: How laser-produced ultra-high current proton beams propagate from their accelerating foil to a high-density target. Learning to control the dynamics of this process (and the limits and potential thereof) will enable a wide range of applications. While the *raison d'etre* of this project and the physics we investigated are of specific interest to inertial fusion energy science, they are also important for a wide range of other HED phenomena, particularly the isochoric heating of materials.

All concepts envisioned for inertial fusion energy (IFE) achieve the necessary high gain ($E_{\text{fusion\_burn}}/E_{\text{target\_driver}}$) by compression of deuterium/tritium (DT) fuel to extremely high density and igniting its fusion burn in a small hotspot. The main-line ignition method, central hot-spot (CHS) ignition, uses shaped, nano-second-long pulsed lasers (or laser-driven x-rays) to compress a hollow shell of HD fuel by a factor >25× and simultaneously to create a hot, lower density core which can ignite the assembly. The advent of powerful sub-picosecond-pulse lasers allowed decoupling those two goals: one ns-long drive (laser, heavy ion, or Z pinch) compresses the fuel and a second, ps-long pulse delivers the energy to ignite the fuel. The original FI concept had the ps-pulse heating the core by using laser-created hot electrons that streamed in from the critical plasma density surface to the dense core. The ion-ignited variant of FI uses the hot electrons as an intermediary; they create a focused stream of ions which in turn create the initial spark. We investigated the use of protons in this role.

Our strategy was to examine the new physics emerging as we added the complexity necessary to use proton beams in an Inertial Fusion Energy (IFE) application. From the starting point of a proton beam accelerated from a flat, isolated foil, we: 1) curved it to focus the beam, 2) attached the foil to a structure, 3) added a side sheath to protect it from the surrounding plasma, and finally 4) studied the proton beam behavior as it passed through a protective end cap into plasma.

We built up, as we proceded, a self-consistent picture of the quasi-neutral plasma jet that is the proton beam that, for the first time, included the role of the hot electrons in shaping the jet. Controlling them — through design of the accelerating surface and its connection to the surrounding superstructure — is critical; their uniform spread across the proton accelerating area is vital, but their presence in the jet opposes focus; the electron flow away from the acceleration area reduces conversion efficiency but can also increase focusing ability. The understanding emerging from our work, and the improved simulation tools we have developed allow designing structures that optimize proton beams for focused heating.

2. Introduction/Background

In high-intensity laser/thin-foil interaction experiments, electrons are accelerated by the laser at the target front surface to relativistic velocities. These electrons travel through the foil to form a sheath field of O(MV/μm) at the rear surface. Such an electric field is large enough to ionize and accelerate layers of material away from the surface, the so-called Target Normal Sheath Acceleration (TNSA) mechanism (Fig. 1) [Hatchett00, Wilks01] for energetic proton and ion production. Ions with the largest charge to mass ratio accelerate fastest and gain the most energy so protons, omnipresent as O(10) nm films barring intensive cleaning procedures, dominate beams created by present laser facilities.

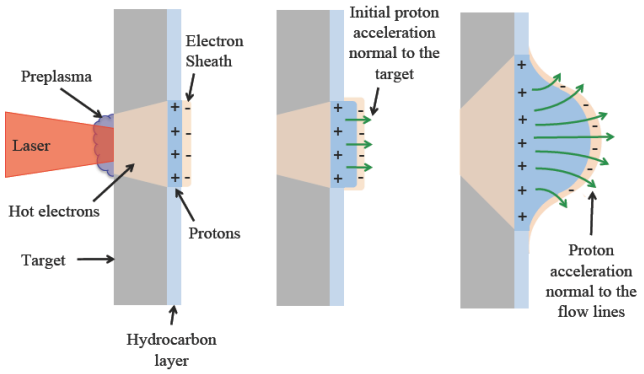

Fig. 1. Schematic picture of proton target normal sheath acceleration: Laser acceleration of protons from the back side of thin foil target initially normal to the target surface and later normal to the flow lines.

The potential value of these proton beams, discovered only a decade ago [Snavely00, Hatchett00], was immediately recognized. They have already found widespread use in High Energy Density (HED) physics laboratories as isochoric heaters [Snavely07, Patel03] that allow study of conditions in, for instance, the interior of Jupiter [Baraffe05], probes of material density [Roth02] and of transient electric and magnetic fields [Borghesi02, Fuchs07, Quinn09] with micron scale resolution [MacKinnon06], for nuclear reactions to create directional neutrons [Lancaster04, Higginson10] and isotope production [Spencer01, Fritzler03], for applications in medicine, material science, and neutron resonance spectroscopy, and they hold promise as the ignitor in Fast Ignition fusion [Roth01, Roth09, Key06] and as a front end to particle beam devices [Cowen04, Fuchs05] for, *e.g.*, tumor treatments [Salamin08, Bulanov02]. The value of these beams comes from the energy of their particles and their ease of production and control. Energies as high as 67MeV are now readily produced [Gaillard11, Offermann11] while new mechanisms for generating even higher energy protons and ions are also being explored [Yin11a,b]. In addition any material covered with a proton rich surface layer (e.g. every surface in almost every experiment) irradiated with a ~picosecond heating pulse, will generate a proton beam normal to its surface by the TNSA mechanism; a curved surface will focus that beam. A thin curved surface can generate a proton beam that focuses ≈10% of the incident laser energy, which can isochorically heat a solid to a higher, more uniform temperature than by direct irradiation of the laser pulse that created the proton beam [Snavely07].

Over the last 12 years investigating the fast ignition concept has proved to be challenging. Injection of the ignition energy involves enough power- and energy-density (I_{Laser}>10^{20}Wcm^{-2}, pressure>Gbar, magnetic field B>100MGauss, electric field E>10^{12}V/m) and large numbers of relativistic particles ($kT_{electron}$>MeV, $I_{electron}$>1GAmp) to enter a new regime—a relativistic high energy density (RHED) plasma—whose properties vary substantially from their less energetic brethren. Experimental access to this regime in a limited way began with operation of the LLNL Nova PW followed, after its retirement, by a number of other lasers. None of these were capable

of providing an RHED environment for research in the FI relevant regime until the recent availability of PW, high energy (>kJ), longer pulse (~10 ps) facilities (OMEGA, OMEGA EP at LLE; LFEX at ILE in Japan). Because of considerable progress over the last few years in understanding the issues critical to the fast ignition concept and advances in predictive modeling capabilities, we have been well positioned to perform expanded experimental efforts on these newer facilities. Our goal was to understand the interplay of forces involved with the creation, injection, and transport of relativistic electrons into HED plasmas. Such scientifically rich understanding with the benchmarked modeling codes has led to our improved capability to extrapolate to FI ignition conditions and evaluate the FI concept.

Section 3 details our progress and accomplishments over the last few years of our Advanced Concept Exploration (ACE) program (started Aug. 2005). Section 4 summarizes the achievements and impacts of the ACE program. A list of PhD theses and scientific papers papers published during the last three years are detailed in Section 5.

3. Progress and Accomplishments

This program is meant to obtain a critical understanding of proton generation and focusing under fast ignition conditions, allowing the evaluation of its attractiveness as an alternative ignition concept. The common understanding at the beginning of our project was that the protons were ballistic particles accelerated perpendicular to their originating surface. That was far too simplistic. We discovered that the hot electrons that do the acceleration also: 1) co-move with protons and oppose tight focus, 2) leak from the accelerating surface causing loss in conversion efficiency, 3) leak into the surrounding structure to reshape the proton beam, and 4) exchange with cold electrons as the jet passes through the protective end cap into the compressed plasma. We describe below the detailed physics of these effects and ways they can be used to our advantage.

3.1. Proton Focus and the Effect of Hot Electrons

Initial proton focusing tests, assuming straight-line path for the protons orthogonal to the starting surface (the common wisdom in those days [Wilks01]) to calculate the location and size of the beam waist gave beam-waists in impossible locations—at less than the radius of curvature or even at negative values. Careful consideration of the proton beam generation mechanism, and experiments to test the effects of different configurations has clarified the situation, shown the complete validity of our measurements, and indicated the focus may be even better than we had predicted [Bartal12].

Experiments were carried out on the Trident laser facility (E=75 J, □=0.6 ps) [Batha08] at LANL. The proton beam was generated from a surface supported by an enclosing structure similar to that envisioned for FI targets (Fig. 2). Partial and fully freestanding hemispherical shell targets were also included for comparison. A thin adsorbed layer of hydrocarbons on the foil surface provided the protons [Foord07].

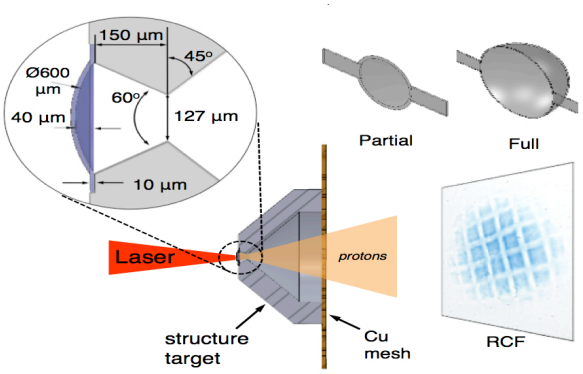

Fig. 2. Experimental setup showing accelerating surface held in a jig that approximates the protective shield.

The focusing characteristics of the beam were determined by imaging the protons through a Cu mesh and recording the mesh pattern on a stack of radiochromic film (RCF) [Nürnberg09]. The 3D ray tracing technique projecting back the shadow of the mesh on the RCF through the original mesh initially assumed straight-line propagation of the protons from the source to the detector. As noted above, that gave nonsensical results.

The generated proton beam was simulated using the hybrid particle-in-cell code LSP [Welch01]. The trajectories for a group of test particles are shown in Fig. 3. After the initial acceleration, protons bend away from the axis. The curved trajectories can be qualitatively understood with a simple model of the radial electric field. Following the initial acceleration phase near the surface, the hot electrons are confined by the ambipolar field of the positively

charged proton beam. The hot-electron pressure gradient sets up a radial electric field, $E_r \approx -\nabla(P_e)/n_e \approx kT_{ehot}/R$, where R is the radial scale length of the beam, kT_{ehot}, P_e, and n_e are the hot electron temperature, pressure, and density, respectively. The radial expansion field thus increases as R decreases. Simulations indicate that the radial field in the beam is of the order of a few MV/100 μm, which is sufficient to deflect a multi-MeV proton over the spatial scale of the target. Depending on the curvature of the trajectories, the inferred focal position determined from extrapolating the trajectories to the axis may fall much inside the actual focal position of the proton beam. That is shown in Fig. 4(a), where the apparent minimum diameter was calculated using a straight-line analysis of LSP-calculated RCF data (which is in excellent agreement with calculations from experimental data), compared to Fig. 4(b), which shows the beam diameter profile determined from the LSP-calculations. The inferred diameter and beam position are both much larger than apparent from the shadows-based calculation [Fig. 4(a)] [Bartal12].

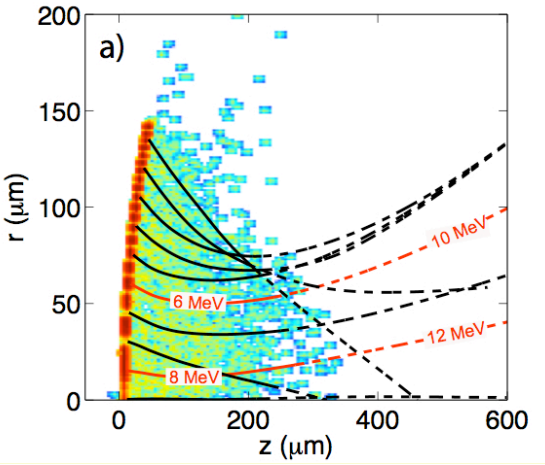

Fig. 3. Proton beam bending by hot electrons for a hemispherical section with 300 μm radius of curvature (a) isolated in space, and (b) encased in an open-ended conical shell.

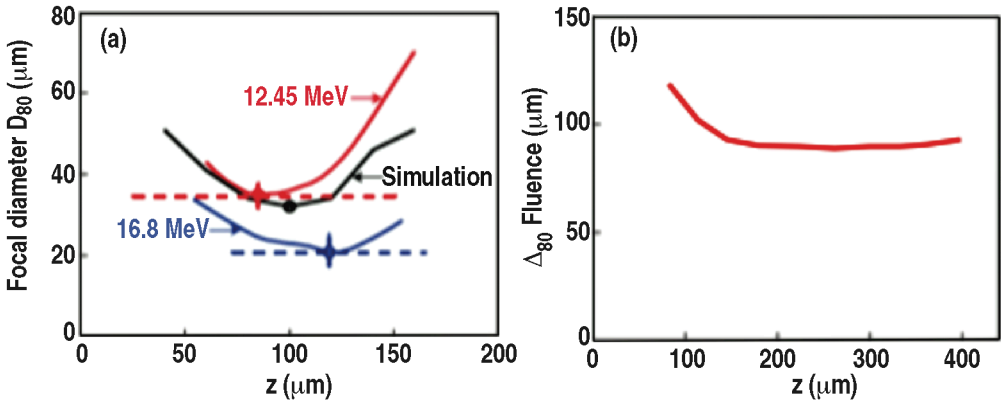

Fig. 4. (a) Comparison of experimental (dashed lines) and simulation results for a freestanding partial hemisphere target. The profile of $D_{80}(z)$ is plotted. The circles, along with the appropriate error bars, represent the minimum D_{80}. The simulation includes all protons with D > 9 MeV. (b) Fluence curve $\Delta_{80}(z)$ for proton energies >3MeV (relevant to FI requirements).

In an IFE application, the region of the proton focus, where the defocus force is strongest, would be outside the protective cone. Since the jet plasma density is lower than the fuel density, one would expect this expansion mechanism to disappear; the fuel electrons can easily cancel the field set up by the jet electrons. We found in Sec. 3.4 the situation was not that simple.

3.2. Hot Electron Confinement for High Conversion Efficiency

We have investigated the effect on laser-to-proton energy conversion efficiency of confining electrons with laser experiments on reduced mass targets (RMT) at the Center for Ultrafast

Optical Science, Univ. of Michigan and with particle-in-cell simulations using the LSP code [Morace13]. Confining electrons to the focusing surface ensures their energy is spent maintaining the sheath fields — maximizing their voltage and extending their lifetime, and should have a dramatic effect on the energy of the resulting proton beam.

Experiments were carried out using the λ=1035 nm, E=5 J, τ=400 fs T-Cubed laser focused to d=20 μm fwhm diameter and I=10^{18} W/cm^2. The targets were 150 μm squares, 10 μm thick Cu attached to the surrounding foil with 4 legs 106 μm long and either 21, 42, or 84 μm wide. In addition 3 mm × 3 mm Cu foil targets were used as comparison. A stack of RCF, digitized with a calibrated scanner was the proton diagnostic. The first two layers were sensitive to proton energies above 1.05 MeV and 3.1 MeV, respectively (Fig. 5). The dependence on leg width is shown quantitatively in Fig. 6.

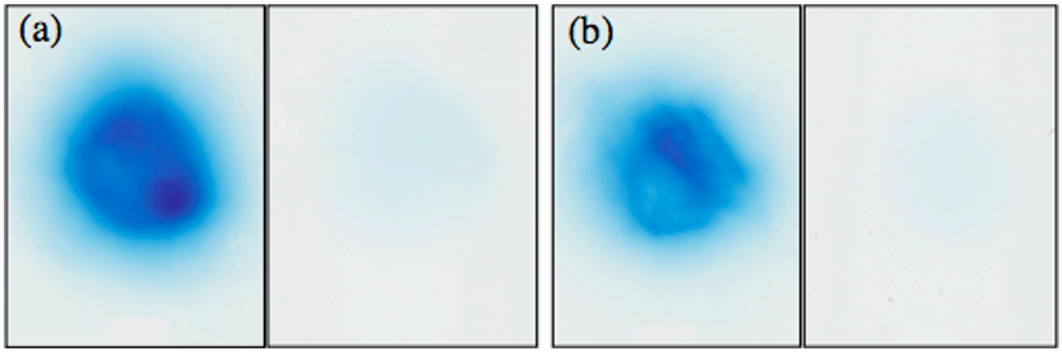

Fig. 5. Collected RCF data for a target with (a) 21 μm leg width and (b) 84 μm leg width. The 21 μm leg 1st RCF data show higher density (dose) compared to that from the corresponding 84 μm leg. In both cases the dose is very low on the 2nd RCF.

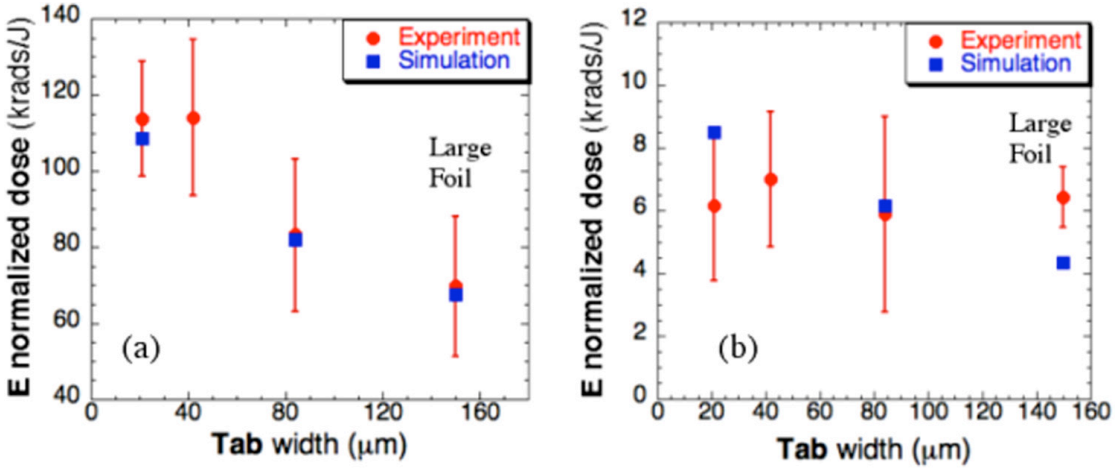

Fig. 6. Energy normalized integrated dose as a function of the RMT leg size. Red color represents the experimental data, blue color the 3D PIC hybrid simulation results. (a) First RCF layer, corresponding to proton energies above 1 MeV. (b) Second RCF layer, corresponding to proton energies above 3.3 MeV. Note the dose here is <1/10 that of the first layer. The 150 m leg size symbolically corresponds to the large Cu foil.

One can qualitatively understand this increase in proton intensity as coming from increasing electron confinement with narrowing RMT legs caused by the diminishing opportunity they present for the hot electrons to escape. Quantitative understanding was pursued with the use of 3D hybrid particle-in-cell (PIC) simulations. Those results are also shown in Fig. 6. We assumed a laser-to-fast-electron conversion efficiency of 30% to calculate the simulated energy-normalized deposited dose. This is consistent with experimentally inferred values [Key98]. For the first RCF, the agreement is excellent. The simulation captures the much lower intensity in the second RCF, but error bars at this low intensity preclude comparing the trend. We then looked within the simulation at the fast electron density $n_e(t)$ and the electric field component $E_z(t)$ to understand the details of the effect of RMT leg width on conversion efficiency and spectra. n_e and E_z are the same for all targets during the laser pulse. It is only at later times (~1.5 ps) that the differences among the target types become evident. As shown in Fig. 7, shortly after the end of the injection, the (radially averaged) fast electron density is larger for more isolated targets [Fig. 7(a)]. In fact, for these highly isolated targets the fast electrons are better confined in the RMT, leading to larger charge density and consequently larger sheath field E_z [Fig. 7(b)]. In poorly isolated targets instead, the fast electrons can spread radially more easily, and the overall charge density is reduced, as well as the amplitude of E_z.

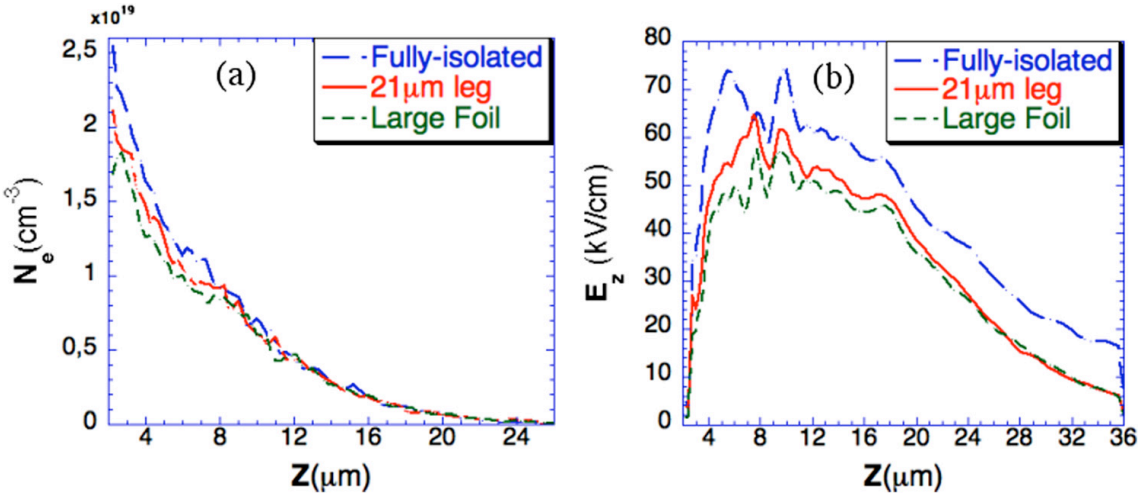

Fig. 7. Fast electron density (a) and E_z component (b), taken at 1.5 ps simulation time (0.5 ps after the injection) and averaged over the RMT surface, as a function of the distance from the target surface. At this time, it is already possible to observe the dependence of proton acceleration on target isolation.

The slower decay of the sheath field in the isolated targets maintains the accelerating field and allows to accelerate of protons more efficiently at later times, showing clear differences in the total kinetic energy.

It is important to mention that the choice of thin legs to isolate the RMT from the support foil is not equivalent to isolating it by means of a dielectric material. The voltages created by the laser-generated hot electrons would generate an ionization wave [Krasheninnikov05] that rapidly crosses the barrier.

Figure 8 shows the time integrated proton kinetic energy as a function of time; it demonstrates how the laser-to-proton conversion efficiency is highly dependent on the target isolation. We observe that even though the initial acceleration stage is similar for all targets, at around 1.4 ps (or 0.4 ps after the end of the injection) the curves start to separate. The acceleration ceases earlier for poorly isolated targets; it continues longer the better the isolation. From the simulation data, it is possible to obtain the integrated doses deposited into the RCFs. The calculation is made accounting for the Bragg curve in the RCF relative to the specific proton energy and is plotted in Fig. 5.

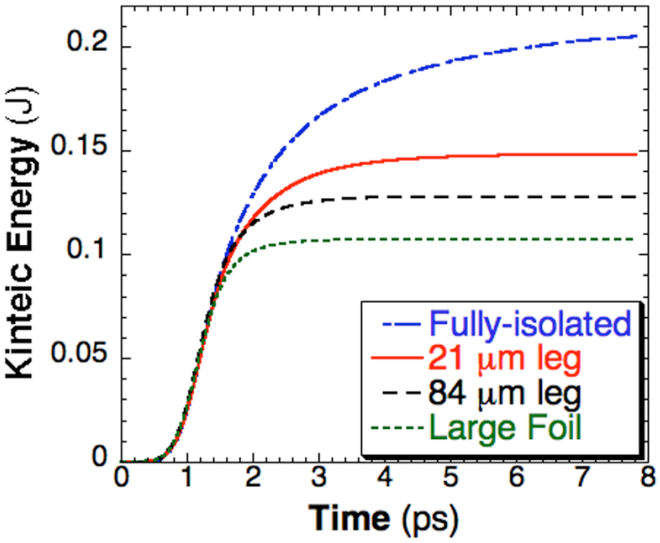

Fig. 8. Proton (forward accelerated) total kinetic energy vs. time, for the four types of targets. The proton acceleration is initially identical. They only start diversifying at about 1.4 ps simulation time, or 0.4 ps after the injection.

Finally, from the simulation data, it is possible to estimate the laser-to-proton conversion efficiency. Considering only the forward-accelerated protons with energy above 1.05 MeV, we find efficiencies of 3%, 2.5%, and 2.1% for the 21 μm leg, 84 μm leg, and large foil cases, respectively. That is, one finds an efficiency increment of ~50% for highly isolated target with respect to large foils.

3.3. Hot Electron Leakage for Proton Focus Control

The structure necessary to support and protect the proton-generating surface plays a major role in the proton beam — more than just an escape route for hot electrons. The Trident experiments referred to in Sec. 3.1 showed that the consequent charging of the surrounding surfaces could also focus the protons. To study that we have used 2D hybrid LSP PIC code [Welch01, Welch06] simulations to self-consistently model the whole structure and its evolution for 15 ps, the time necessary for protons to reach their asymptotic velocities [Qiao13].

The simulations cover 400 μm transversely and 700 μm longitudinally with zero potential, perfect conducting, perfectly absorbing boundary on all sides excepting the laser entry surface. Collisions are included based on Spitzer collision frequencies. A 1 μm wavelength laser with peak intensity I_o= 4×10^{19}W cm^{-2} and Gaussian distribution with r_o=45 μm enters from the left boundary (z=-50 μm and irradiates the target at z=0. The laser pulse has a trapezoidal temporal profile of total duration 500 fs including rise and fall of 50 fs each. Three geometries of carbon targets were modeled: planar foil, open-hemisphere, and hemisphere-cone targets, using the ion charge states of C^{4+}, mass density 2.7 g/cm^3, and thickness of 10 μm. The partial hemispheres have a radius of curvature of 300 μm and diameter 300 μm. The cone structure is taken as Al^{10+}. A preplasma is assumed in each case with scale length L=4 μm, and all other surfaces are coated with a 50 nm hydrocarbon contamination layer.

The hot electrons propagate nearly ballistically in the thin low-Z carbon target until they reach the rear surface. It can be seen in Fig. 9(a,d), and 9(g), at t = 600 fs when the laser pulse is just over, that only a tiny fraction of the hot electrons (those in the high energy tail up to 28 MeV) can escape far away into vacuum. Their escape sets up a strong sheath potential. Lower energy electrons reflect from this sheath and, retaining their transverse motion, spread across the target. In the 600 fs pulse duration they spread ~150 μm, but extend from the cold surface (before the protons start to move) only ~10 μm.

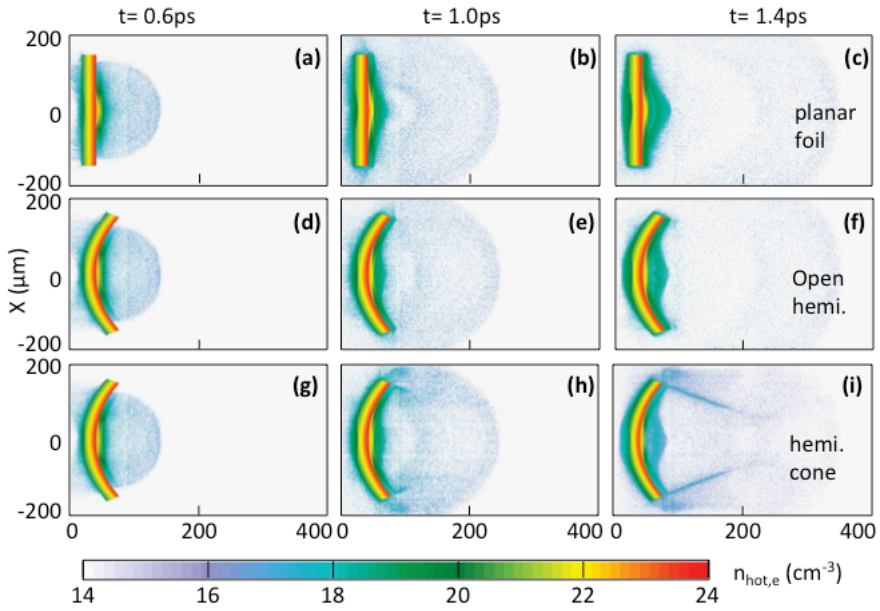

Fig. 10. Hot-electron density maps at t = 0.6, 1.0, and 1.4 ps produced from (a-c) planar-foil, (d-f) open-hemisphere, and (g-i) hemisphere-cone targets, by a laser pulse with I=4×10^{19} W cm^{-2} and τ=600 fs.

Because the smallest plasma scale length direction initially is normal to the target surface direction (see [Qiao13] for detailed discussion), the sheath electric field and proton acceleration are, initially, dominantly along the direction normal to the target rear surface. For the curved hemisphere targets, the electric field has a stronger transverse component E_x, shown in Fig. 11(d), Fig. 11(g) leading, in principle, to geometrical focusing of protons initially expected for TNSA.

However, after protons are accelerated into vacuum, they form, together with the co-moving hot electrons, a quasi-neutral plasma jet undergoing thermal expansion driven both longitudinally and transversely by the local hot-electron pressure. During this thermal expansion stage, proton acceleration and focusing behaviors depend heavily on the hot-electron dynamics, which is significantly influenced by the target geometries, particularly by the surrounding cone structure, into which a significant fraction of the hot electrons can leak [Fig. 11(h,i)]. In particular, the longitudinal sheath electric field E_z together with the magnetic field B_y, induced by the density gradient between the target rear surface and the vacuum, confine a number of hot electrons to flow along the target rear surface, forming a surface current similar to those in the electron FI

scheme. This surface current can be maintained along the cone wall for the hemisphere-cone target, as seen in Fig. 10(h,i) and Fig. 11(h,i).

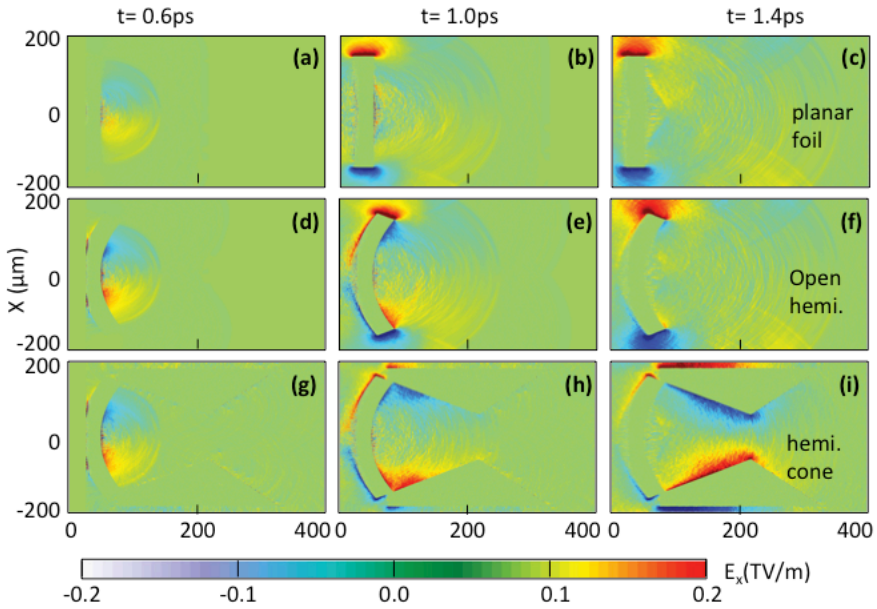

Fig. 11. The transverse electric field E_x at times t = 0.6, 1.0, and 1.4 ps for (a-c) planar-foil, (d-f) open-hemisphere, and (g-i) hemisphere-cone targets, where laser and target parameters are the same as in Fig. 10.

The above complex hot-electron dynamics leads to different proton focusing dynamics depending on the target geometries. For the planar-foil target, the surface current mentioned above disappears rapidly after protons expand into vacuum. The hot-electron thermal pressure in the plasma is higher close to the laser axis with gradient directed transversely outward due to the finite laser focus, resulting in a spreading of the proton beam. For the open-hemisphere target, the surface current can be maintained for a longer distance in the z direction along the curved surface, and the transverse component of the sheath field E_x can be maintained out to z~100 μm Fig. 11(e)] (E_x also diffuses from the surface into the vacuum significantly) for proton focusing. Beyond this the sign of E_x changes [Fig. 11(f)) due to the hot-electron pressure gradient in the expanding plasma, which bends the proton trajectories and limits the achievable focus as discussed in Sec. 3.1.

However, for the hemisphere-cone target case, the hot-electron flow is guided and continued along the cone wall surface, maintaining the focusing electric sheath field sign up to the cone tip, as shown in Figs 11(h,i). This focusing field diffuses inward significantly from the wall surface into the vacuum, therefore a significant enhanced focusing of proton beams is achieved, although the hot-electron current is only along the wall surface.

You can see the results of these fields in the proton density maps for the different geometries (Fig. 12).

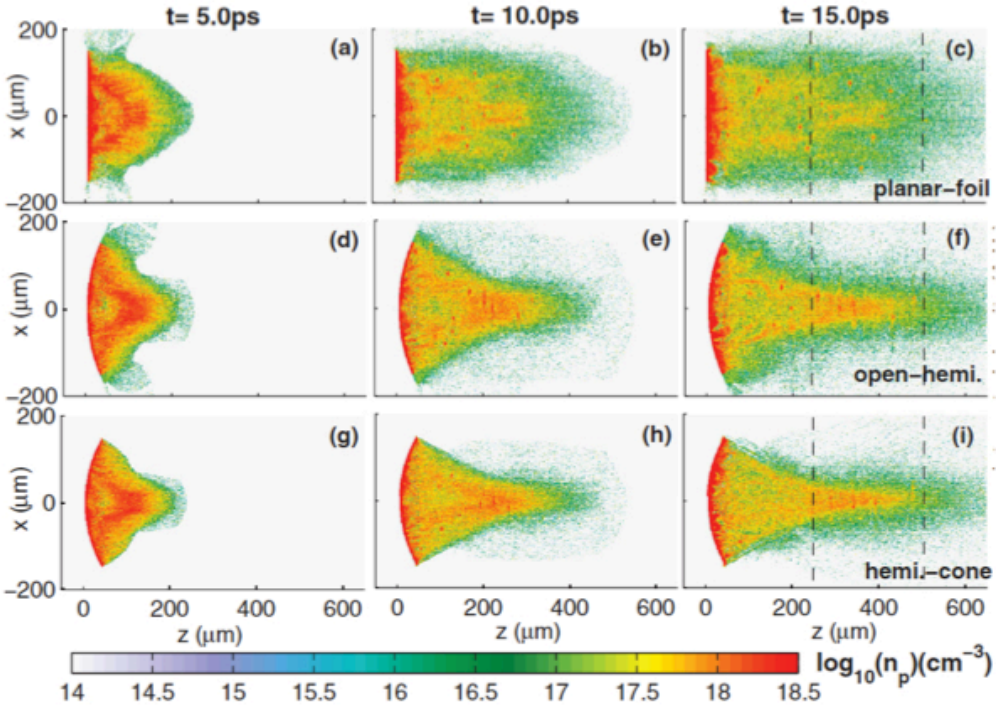

Fig. 12. Proton density maps at t = 5.0, 10.0, and 15.0 ps from (a-c) planar-foil, (d-f) open-hemisphere, and (g-i) hemisphere-cone targets.

Cross-sections through the beams integrated between the dashed lines in (c), (f), and (i), are shown in Fig. 13. A clear enhanced focusing — about 15% reduction in the focal radius, can be seen for the hemisphere cone relative to the open hemisphere target.

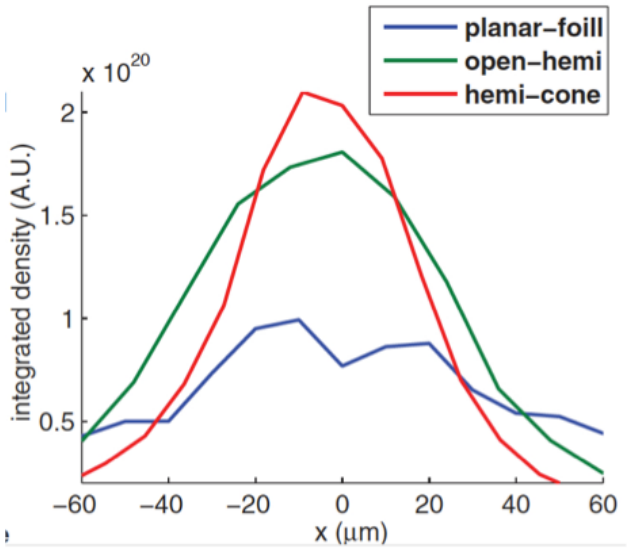

Fig. 13. Transverse profiles of the proton density at t = 15.0 ps integrated between the dashed lines in Fig. 3-9(c), (f), and (i), for planar-foil, open-hemi, and hemi-cone, respectively.

3.4. Proton Jet Transport Dynamics in Dense Plasma

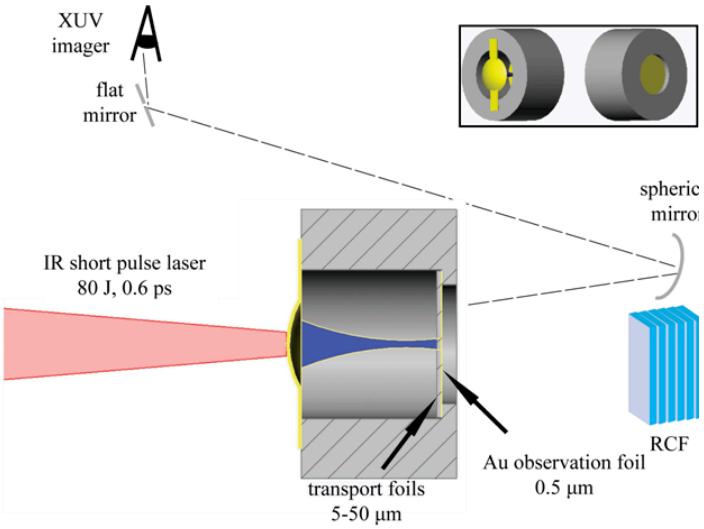

Fig. 14. Experimental setup for examining proton transport into dense plasma. The beam diameter at the back surface was characterized by imaging its thermal emission at 68 eV. The proton beam was characterized using an RCF film stack.

All of the above experiments and simulations have examined the proton beam as it expanded from its source out into vacuum. For use in an IFE application, the beam must, well before focus, transit a protective end cap (a high-Z dense plasma) and enter the compressed fuel. We recently designed an experimental campaign to examine that transition. The experiment (Fig. 14) was conducted with the Trident laser (E=75 J, □=0.6 ps) at LANL. Protons from a laser-irradiated spherically curved target foil were focused into a planar transport foil of varied atomic number (Z) and thickness. The transport foil was positioned so that its rear, Au-coated surface coincided with the expected focal position of the beam (510 μm). XUV emission brightness depends strongly on temperature of the surface with detectable emission indicating that the surface locally reached >20 eV. It was thought that the hot-electron transverse force would be absent for the time traversing the transport foil, and the beam diameter at its rear surface correspondingly reduced. The stopping power of the transport foils was set to preferentially observe either 1 or 1.9 MeV protons (their Bragg peak should occur just at the back surface). We examined the effects for a variety of foil thicknesses from 5 to 50 μm, modifying the Z (CH, Al, Cu, Au) (except for the 0.5 μm Au back surface) to maintain a constant stopping power. In this view, the observed beam diameter should decrease with increasing foil thickness (decreasing Z).

However, the beam diameter (roughly) decreased with increasing Z, with the thin Cu and Au transport foil targets producing very tightly confined emission profiles (~44 μm) compared to the Al and CH cases (~180 μm) (Fig. 15). This variation with material (Fig. 16) indicates a clear dependence of the beam transport and heating dynamics on the target material properties that had not been accounted for, and which was not included in our codes. For example, Monte Carlo calculations in a cold target suggest that straggling can only account for a ~10 μm difference in beam expansion for protons traversing these foils and that expansion would be greatest for the highest areal density targets [Ziegler10].

To correctly model this beam-plasma interaction, a new ion stopping-power calculation module [Kim13, McGuffey13] covering both the warm and hot dense plasma regimes has been implemented in the hybrid particle-in-cell code LSP, where both the contributions from bound and free electrons are taken into account for the total stopping power, but not including the nuclear term; that is insignificant for these plasmas (1).

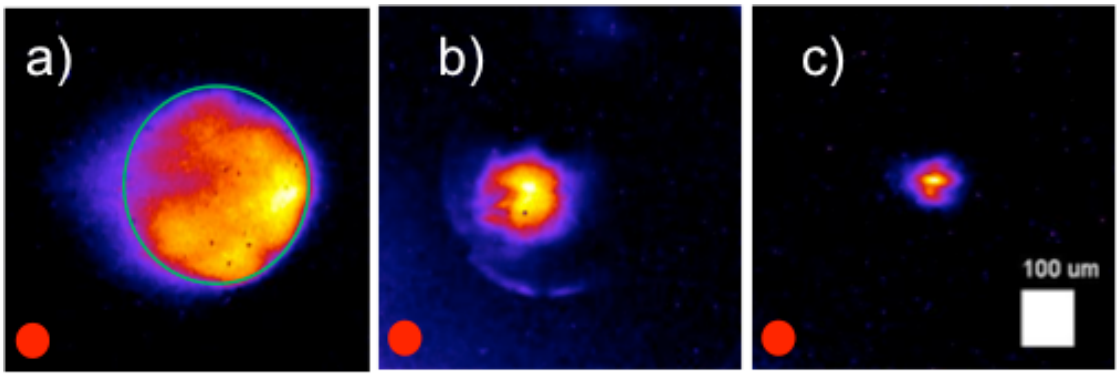

Fig. 15. 68 eV XUV emission from (a) the accelerating foil, and (b) CH (50 μm thick) and (c) Au (12.5 μm thick) transport foils. The red circle is the diameter of the focused laser beam.

$$(-\frac{dE}{dX})plasma = (-\frac{dE}{dx})bound + (-\frac{dE}{dX})free + (-\frac{dE}{dx})nuclear \quad (1)$$

The ion stopping power of the target depends on the balance of these two terms. They in turn depend on the local temperature and ionization level, which can vary significantly in space and time as the beam deposits energy. The range of ions and target heating profile can therefore be substantially altered from the predictions of standard stopping models, i.e. with the rising ionization during the interaction, stopping power decreases for particles at the low-energy range but increases for energies above ~1 MeV. In the LSP code, these effects are now included self-consistently: The Bethe formula with a shell correction was implemented into the code for bound electronic stopping power and the free electron gas model with plasma dielectric function was used for free electron stopping. The ionization state is updated locally and dynamically using an equation of state table. The stopping power module has been benchmarked against the latest theoretical plasma stopping calculations [Faussurier10].

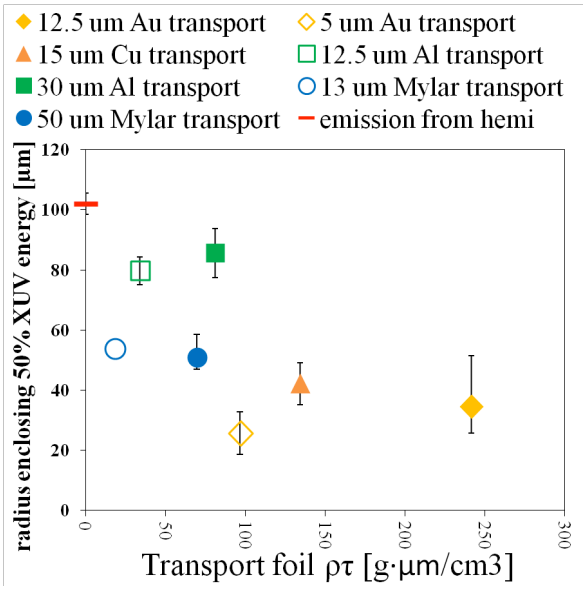

Fig. 16. Size (fwhm) of the beam-heated region for a variety of transport foils. The size varied weakly for foils of the same material (color) but different thickness (filling), as expected, but varied dramatically with material.

Using this new modeling tool, we have the capability for the first time to study the generation of laser-accelerated ion beams and their propagation in vacuum and transport and deposition in warm dense plasmas. We have systematically studied the dependences of these interactions on the beam intensity, target material and initial target plasma temperature [Kim13]. It was found that particle ranges can as much as double in the plasmas we investigated, compared to a cold target case and protons can be further focused (Fig. 17). These effects depend strongly on material.

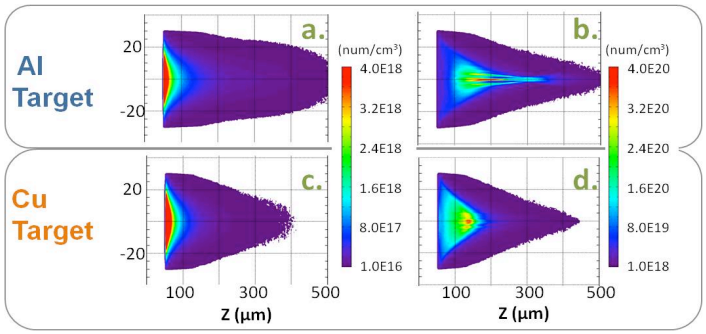

Fig. 17. Proton density image at t = 12ps when a proton beam with Maxwellian energy distribution of slope 5 MeVand pulse length 4 ps is injected and fully stopped in Al and Cu target of initial temperature 10 eV, where the beam current density is respectively (a) and (c): 1×10^{9}, (b) and (d): 1×10^{11} A/cm^2.

4. Overall Summary and Impact

This work has systematically investigated all of the components necessary for proton ignited FI. At each stage we have developed experimental platforms and added new modules to the simulation codes to gain — for the first time — complete and self-consistent understanding of the physics involved. Our findings include:

- The achievable focus of proton beams in vacuum is limited by the thermal pressure gradient in the laser-generated hot electrons that drive the process. This bending can be suppressed using a controlled flow of hot electrons along the surrounding cone wall, which induces a local transverse focusing sheath electric field. The resultant (vacuum-focused) spot can meet IFE requirements.
- Confinement of laser-generated electrons to the proton accelerating area can be achieved by supporting targets on thin struts. That increases laser-to-proton conversion energy by ~50%. As noted above, confinement should not be total; necessary hot-electron leakage into the surrounding superstructure for proton focusing can be controlled by with the strut width/number.
- Proton jets are further modified as they enter the fuel through the superstructure's end cap. They ionize the material, changing its stopping power, and generate currents during that transit that can further focus the proton beams. We developed a new ion stopping module for LSP code that properly accounted for changes in stopping power with ionization (e.g. temperature), and will be using it in future studies.
- The improved understanding, new experimental platforms, and the self-consistent modeling capability allow researchers a new ability to investigate the interaction of large ion currents with warm dense matter. That is of direct importance to the creation and investigation of all aspects of warm dense matter as well as to proton-ignited FI.

5. Project Staff Over the Period of Contract

5.1. General Atomics

Dr. R.B. Stephens – P.I.
Dr. K.U. Akli
Dr. M.S. We

5.2. University of California San Diego

Prof. F.N. Beg
T. Bartal – graduate student
J. Kim – graduate student
Dr. C. Bellei – post-doctoral fellow
Dr. B. Qiao – Research Scientist
C. McGuffey – post-doctoral fellow

5.3. The Ohio State University

Prof. L. Van Woerkom
Prof. R.R. Freeman
D. Wertepny – graduate student

5.4. Lawrence Livermore National Laboratory

Dr. M.E. Foord – P.I.
Dr. M.H. Key
Dr. A.J. Mackinnon
Dr. S. LePape
Dr. P.K. Patel
Dr. H.S. McLean

6. References

[Baraffe05] I. Baraffe, "Structure and evolution of giant planets," *Space Sci. Rev.* **116**, 67 (2005).

[Bartal12] T. Bartal, M.E. Foord, C. Bellei, M.H. Key, K.A. Flippo, S.A. Gaillard, D.T. Offermann, P.K. Patel, L.C. Jarrott, D.P. Higginson, M. Roth, A. Otten, D. Kraus, R.B. Stephens, H.S. McLean, E.M. Giraldez, M.S. Wei, D.C. Gautier, F.N. Beg, "Focusing of short-pulse high-intensity laser-accelerated proton beams," *Nature Phys.* **8**, 139 (2012).

[Batha08] S. Batha, R. Aragonez, and F. Archuleta, "TRIDENT high-energy-density facility experimental capabilities and diagnostics," *Rev. Sci. Instrum.* **79**, 10F305 (2008).

[Borghesi02] M.J. Borghesi, *et al.*, "Propagation issues and energetic particle production in laser-plasma interactions at intensities exceeding 10^{19} W/cm^2," *Laser and Part. Beams* **20**, 31 (2002).

[Borghesi04] M. Borghesi, *et al.*, "Multi-MeV proton source investigations in ultra-intense laser-foil interactions," *Phys. Rev. Lett.* **92**, 055003 (2004).

[Bulanov02] S.V. Bulanov, *et al.*, "Generation of high-quality charged particle beams during the acceleration of ions by high-power laser radiation," *Plasma Phys. Rep.* **28**, 975 (2002).

[Cowan04] T.E. Cowan, *et al.*, "Ultralow emittance, multi-MeV proton beams from a laser virtual-cathode plasma accelerator," *Phys. Rev. Lett.* **92**, 204801 (2004).

[Faussurier10] G. Faussurier, C. Blancard, P. Cossé, P. Renaudin, "Equation of state, transport coefficients, and stopping power of dense plasmas from the average-atom model self-consistent approach for astrophysical and laboratory plasmas," *Phys. Plasmas* **17**, 052707 (2010).

[Foord07] M.E. Foord, P.K. Patel, A.J. MacKinnon, S.P. Hatchett, M.H. Key, B. Lasinski, R.P.J. Town, M. Tabak, S.C. Wilks, "MeV proton generation and efficiency from an intense laser irradiated foil," *High Energy Dens. Phys.* **3**, 365 (2007).

[Fritzler03] S. Fritzler, *et al.*, "Proton beams generated with high-intensity lasers: Applications to medical isotope production," *Appl. Phys. Lett.* **83**, 3039 (2003).

[Fuchs05] J. Fuchs, *et al.*, "Ultra-low emittance proton beams from a laser-virtual cathode plasma accelerator," *AIP Conf. Proc.* **737**, Vol. 1, 942 (2005).

[Fuchs07] J. Fuchs, *et al.*, "Comparative spectra and efficiencies of ions laser-accelerated forward from the front and rear surfaces of thin solid foils," *Phys. Plasmas* **14**, 053105 (2007).

[Gaillard11] S.A. Gaillard, *et al.*, "Increased laser-accelerated proton energies via direct laser-light-pressure acceleration of electcrons in microcone targets," *Phys. Plasmas* **18**, 056710 (2011).

[Hatchett00] S.P. Hatchett, *et al.*, "Electron, photon, and ion beams from the relativistic interaction of Petawatt laser pulses with solid targets," *Phys. Plasmas* **7**, 2076 (2000).

[Higginson10] D.P. Higginson, J.M. McNaney, D.C. Swift, T. Bartal, D.S. Hey, R. Kodama, S. Le Pape, A. Mackinnon, D. Mariscal, H. Nakamura, N. Nakanii, K.A. Tanaka, F.N. Beg, "Laser generated neutron source for neutron resonance spectroscopy," *Phys. Plasmas* **17**, 1000701 (2010).

[Key98] M.H. Key, M.D. Cable, T.E. Cowan, K.G. Estabrook, B.A. Hammel, S.P. Hatchett, E.A. Henry, D.E. Hinkel, J.D. Kilkenny, J.A. Koch, W.L. Kruer, A.B. Langdon, B.F. Lasinski, R.W. Lee, B.J. MacGowan, A. MacKinnon, J.D. Moody, M.J. Moran, A.A.

Offenberger, D.M. Pennington, M.D. Perry, T.J. Phillips, T.C. Sangster, M.S. Singh, M.A. Stoyer, M. Tabak, G.L. Tietbohl, M. Tsukamoto, K. Wharton, and S.C. Wilks, "Hot electron production and heating by hot electrons in fast ignitor research," *Phys. Plasmas* **5**, 1966 (1998).

[Key06] M.H. Key, *et al.*, "Proton fast ignition," *Fusion Sci. & Technol.* **49**, 440 (2006).

[Kim13] J. Kim, B. Qiao, C. McGuffey, M.S. Wei, R.B. Stephens, M.E. Foord, F.N. Beg, "Computational study of self consistent transport and stopping of a laser-driven proton beam in warm dense targets," High Power Laser Workshop, Menlo Park, CA, 1-2 October 2013.

[Krasheninnikov05] S.I. Krasheninnikov, A.V. Kim, B.K. Frolov, R. Stephens, "Intense electron beam propagation through insulators: Ionization front structure and stability," *Phys. Plasmas* **12**, 073105 (2005).

[Lancaster04] K.L. Lancaster, S. Karsch, H. Habara, F.N. Beg, E.L. Clark, R. Freeman, M.H. Key, J.A. King, R. Kodama, K. Krushelnick, K.W.D. Ledingham, R. McKenna, C. Murphy, P.A. Norreys, R. Stephens, C. Stöeckl, Y. Toyama, M.S. Wei, M. Zepf, "Characterization of ^{7}Li(p,n)^{7}Be neutron yields from laser produced ion beams for fast neutron radiography," *Phys. Plasmas* **11**, 3404 (2004).

[MacKinnon06] A.J. MacKinnon, *et al.*, "Proton radiography of a laser-driven implosion," *Phys. Rev. Lett.* **97**, 045001 (2006).

[McGuffey13] C. McGuffey, B. Qiao, "Transport of high intensity laser-driven proton beams in solid-density isochorically heated matter," *Proc. of 8th International Fusion Sciences and Applications, Nara Japan*, 11 September 2013.

[Morace13] A. Morace, C. Bellei, T. Bartal, L. Willingale, J. Kim, A. Maksimchuk, K. Krushelnick, M.S. Wei, P.K. Patel, D. Batani, N. Piovella, R.B. Stephens, and F.N. Beg, "Improved laser-to-proton conversion efficiency in isolated reduced mass targets," *Appl. Phys. Lett.* **103**, 054102 (2013).

[Nakamura04] T. Nakamura, S. Kato, H. Nagatomo, and K. Mima, "Surface-magnetic-field and fast-electron current-layer formation by ultraintense laser radiation," *Phys. Rev. Lett.* **93**, 265002 (2004).

[Nürnberg09] F. Nu¨rnberg, *et al.*, "Radiochromic film imaging spectroscopy of laser-accelerated proton beams," *Rev. Sci. Instrum.* **80**, 033301 (2009).

[Offermann11] D.T. Offermann, K.A. Flippo, J. Cobble, M.J. Schmitt, S.A. Gaillard, T. Bartal, D.V. Rose, D.R. Welch, M. Geissel, M. Schollmeier, "Characterization and focusing of light ion beams generated by ultra-intensely irradiated thin foils at the kilojoule scale," *Phys. Plasmas* **18**, 056713 (2011).

[Patel03] P.K. Patel, A.J. Mackinnon, M.H. Key, T.E. Cowan, M.E. Foord, M. Allen, D.F. Price, H. Ruhl, P.T. Springer, and R. Stephens, "Isochoric heating of solid-density matter with an ultrafast proton beam," *Phys. Rev. Lett.* **91**, 125004 (2003).

[Qiao13] B. Qiao, M.E. Foord, M.S. Wei, R.B. Stephens, M.H. Key, H. McLean, P.K. Patel, F.N. Beg, "Dynamics of high-energy proton beam acceleration and focusing from hemisphere-cone targets by high-intensity lasers," *Phys. Rev. E* **87**, 013108 (2013).

[Quinn09] K. Quinn, P.A. Wilson, C.A. Cecchetti, B. Ramakrishna, L. Romagnani, G. Sarri, L. Lancia, J. Fuchs, A. Pipahl, T. Toncian, O. Willi, R.J. Clarke, D. Neely, M. Notley, P. Gallegos, D.C. Carroll, M.N. Quinn, X.H. Yuan, P. McKenna, T.V. Liseykina, A. Macchi, M. Borghesi, "Laser-driven ultrafast field propagation on solid surfaces," *Phys. Rev. Lett.* **102**, 194801 (2009).

[Roth01] M. Roth, T.E. Cowan, M.H. Key, S.P. Hatchett, C. Brown, W. Fountain, J. Johnson, D.M. Pennington, R.A. Snavely, S.C. Wilks, K. Yasuike, H. Ruhl, F. Pegoraro, S.V. Bulanov, E.M. Campbell, M.D. Perry, and H. Powell, "Fast ignition by intense laser-accelerated proton beams," *Phys. Rev. Lett.* **86**, 436 (2001).

[Roth02] M. Roth, M. Allen, P. Audebert, A. Blazevic, E. Brambrink, T.E. Cowan, J. Fuchs, J.C. Gauthier, M. Geißel, M. Hegelich, S. Karsch, J. Meyer-ter-Vehn, H. Ruhl, T. Schlegel, R.B. Stephens, "The generation of high-quality, intense ion beams by ultra-intense lasers," *Plasma Phys. Control. Fusion* **44**, B99 (2002).

[Roth09] M. Roth, "Review on the current status and prospects of fast ignition in fusion targets driven by intense, laser generated proton beams," *Plasma Phys. Control. Fusion* **51**, 014004 (2009).

[Salamin08] Y.I. Salamin, Z. Harman, C.H. Keitel, "Direct high-power laser acceleration of ions for medical applications," *Phys. Rev. Lett.* **100**, 155004 (2008).

[Snavely00] R.A. Snavely, M.H. Key, S.P. Hatchett, T.E. Cowan, M. Roth, T.W. Phillips, M.A. Stoyer, E.A. Henry, T.C. Sangster, M.S. Singh, S.C. Wilks, A. MacKinnon, A. Offenberger, D.M. Pennington, K. Yasuike, A.B. Langdon, B.F. Lasinski, J. Johnson, M.D. Perry, and E.M. Campbell, "Intense high-energy proton beams from petawatt-laser irradiation of solids," *Phys. Rev. Lett.* **85**, 2945 (2000).

[Snavely07] R.A. Snavely, *et al.*, "Laser generated proton beam focusing and high temperature isochoric heating of solid matter," *Phys. Plasmas* **14**, 092703 (2007).

[Spencer01] I. Spencer, *et al.,* "Laser generation of proton beams for the production of short-lived radioisotopes," *Nucl. Instrum. & Methods in Phys. Research B* **183**, 449 (2001).

[Welch01] D.R. Welch, D.V. Rose, B.V. Oliver, and R.E. Clark, "Simulation techniques for heavy ion fusion chamber transport," *Nucl. Instrum. Methods A* **464**, 134 (2001).

[Welch06] D.R. Welch, D.V. Rose, M.E. Cuneo, R.B. Campbell, T.A. Melhorn, "Integrated simulation of the generation and transport of proton beams from laser-target interaction," *Phys. Plasmas* **13**, 063105 (2006).

[Wilks01] S.C. Wilks, A.B. Langdon, T.E. Cowan, M. Roth, M. Singh, S. Hatchett, M.H. Key, D. Pennington, A. Mackinnon, and R.A. Snavely, " Energetic proton generation in ultra-intense laser-solid interactions," *Phys. Plasmas* **8**, 542 (2001).

[Yin11a] L. Yin, *et al.*, "Three-dimensional dynamics of breakout afterburner ion acceleration using high-contrast short-pulse laser and nanoscale targets," *Phys. Rev. Lett.* **107**, 045003 (2011).

[Yin11b] L. Yin, *et al.*, "Mono-energetic ion beam acceleration in solitary waves during relativistic transparency using high-contrast circularly polarized short-pulse laser and nanoscale targets," *Phys. Plasmas* **18**, 053103 (2011).

[Ziegler10] J.F. Ziegler, M.D. Ziegler, and J.P. Biersack, "SRIM – The stopping and range of ions in matter (2010)," *Nucl. Instrum. and Methods in Physics Research B: Beam Interactions with Materials and Atoms* **268**, 1818 (2010).

7. Publications, Presentations, and Theses Since Inception

7.1. Invited Talks

- M.E. Foord, *et al.*, "Simulations and experiments of proton generation and focusing from intense laser irradiation of enclosed targets in fast-ignition cone geometry," International Fast Ignition Workshop, Shanghai, China, 2010.
- M.E. Foord, "Generation and focusing of short pulse high intensity laser accelerated protons," 53rd Annual APS-DPP Meeting, 8 Nov. 2011.
- M.E. Foord, T. Bartal, C. McGuffey, M.S. Wei, B. Qiao, C. Bellei, M.H. Key, P.K. Patel, L.C. Jarrott, D.P. Higginson, R.B. Stephens, and F.N. Beg, "Particle transport and electric fields in a laser-generated focused proton beam," ICOPS 2012, Faro, Portugal, September 2012.
- F.N. Beg, *et al.*, "Dynamics of short pulse high intensity laser produced energetic proton beams," ICOPS 2012, Faro, Portugal, September 2012.
- B. Qiao, "Acceleration and transport of a focused laser-generated proton beams for fast-ignition, " ICOPS, San Francisco, 2013.
- C. McGuffey, "Computational study of transport and stopping of a laser-accelerated proton beam in solid targets," CLEO Pacific Rim, Kyoto Japan, 2 July 2013.
- B. Qiao, C. McGuffey, "Transport of high intensity laser-driven proton beams in solid-density, isochorically heated matter," The 8th International Conference on Inertial Fusion Sciences and Applications, Nara, Japan, 11 September, 2013.

7.2. Contributed Presentations

2010

- T. Bartal, *et al.*, "The effect of hemispherical target diameter on proton focusing." 52nd APS-DPP Meeting, Chicago, Illinois, 8-12 November 2010.
- C. Bellei, *et al.*, "LSP simulations of proton-driven fast ignition," 52nd APS-DPP Meeting, Chicago, Illinois, 8-12 November 2010.
- C. Bellei, *et al.*, "LSP simulations of proton-driven fast ignition," 11th International Workshop on Fast Ignition of Fusion Targets, Shanghai, China, 18-21 October 2010.
- C. Bellei, *et al.*, "LSP simulations of proton-driven fast ignition," Japan-US Fast Ignitor and High Energy Density Workshop, Wakayama Japan, 23-24 October 2010.

2011

- T. Bartal, *et al.*, "Focusing of laser accelerated proton beams from a novel cone shaped target." 7th International Fusion Sciences and Applications, Bordeaux France, 12-16 September 2011.
- C. Bellei, *et al.*, "Focusing of laser-accelerated protons for fast ignition studies," 38th International Conference on Plasma Science and 24th Symposium on Fusion Engineering, 26-30 June 2011.

- A. Morace, *et al.*, "Improved laser to proton energy conversion efficiency in reduced mass targets." 7th International Fusion Sciences and Applications, Bordeaux France, 12-16 September 2011.

2012

- C. McGuffey, *et al.*, "Focusing proton beams into solid-density matter for fast ignition," 24th IAEA Fusion Energy Conf., San Diego, California, October 2012.
- B. Qiao, M.E. Foord, R.B. Stephens, M.S. Wei, P. Patel, H. McLean, M. Key and F.N. Beg, "Dynamics of high-energy proton beam acceleration and focusing from advanced hemisphere-cone target by high-intensity lasers," 54th APS-DPP Meeting, Providence, Rhode Island, 29 October through 2 November 2012.
- C. McGuffey, *et al.*, "Material dependence on transport of high-charge proton beams," 54th APS-DPP Meeting, Providence, Rhode Island, 29 October through 2 November 2012.

2013

- J. Kim, B. Qiao, C. McGuffey, F.N. Beg, M. Wei, R.B. Stephens, M.E. Foord, P.K Patel, H. McLean, "Computational study of transport and stopping of a laser-accelerated proton beam in solid targets," 55th APS-DPP Meeting, Denver, Colorado 11-15 November 2013.
- C. McGuffey, B. Qiao, "Transport of high intensity laser-driven proton beams in solid-density isochorically heated matter," 8th International Fusion Sciences and Applications, Nara, Japan, 11 September 2013.
- J. Kim, B. Qiao, C. McGuffey, M.S. Wei, R.B. Stephens, M.E. Foord, F.N. Beg, "Computational study of self consistent transport and stopping of a laser-driven proton beam in warm dense targets," High Power Laser Workshop, Menlo Park, California, 1-2 October 2013.

7.3. Publications

2011

- T. Bartal, K.A. Flippo, S.A. Gaillard, D.T. Offermann, M.E. Foord, C. Bellei, P.K. Patel, M.H. Key, R.B. Stephens, H.S. McLean, L.C. Jarrott, F.N. Beg, "Proton focusing characteristics relevant to fast ignition," *IEEE Trans. on Plasma Sci.* **39**, 2818 (2011).

2012

- T. Bartal, M.E. Foord, C. Bellei, M.H. Key, K.A. Flippo, S.A. Gaillard, D.T. Offermann, P.K. Patel, L.C. Jarrott, D.P. Higginson, M. Roth, A. Otten, D. Kraus, R.B. Stephens, H.S. McLean, E.M. Giraldez, M.S. Wei, D.C. Gautier, F.N. Beg, "Focusing of short-pulse high-intensity laser-accelerated proton beams," *Nature Phys.* **8**, 139 (2012).
- C. Bellei, M.E. Foord, T. Bartal, M.H. Key, H.S. McLean, P.K. Patel, R.B. Stephens, F.N. Beg, "Electron and ion dynamics during the expansion of a laser-heated plasma under vacuum," *Phys. Plasmas* **19**, 033109 (2012).
- M.E. Foord, T. Bartal, C. Bellei, M. Key, K. Flippo, R.B. Stephens, P.K. Patel, H.S. McLean, L.C. Jarrott, M.S. Wei, F.N. Beg, "Proton trajectories and electric fields in a laser-accelerated focused proton beam," *Phys. Plasmas* **19**, 056702 (2012).

2013

- J.C. Fernández, B.J. Albright, F.N. Beg, M.E. Foord, B.M. Hegelich, J.J. Honrubia, M. Roth, R.B. Stephens, and L. Yin, "Fast ignition with laser driven proton and ion beams," to be published in *Nuclear Fusion* 2013.
- B. Qiao, M.E. Foord, M.S. Wei, R.B. Stephens, M.H. Key, H. McLean, P.K. Patel, F.N. Beg, "Dynamics of high-energy proton beam acceleration and focusing from hemisphere-cone targets by high-intensity lasers," *Phys. Rev. E* **87**, 013108 (2013).
- A. Morace, C. Bellei, T. Bartal, L. Willingale, J. Kim, A. Maksimchuk, K. Krushelnick, M.S. Wei, P.K. Patel, D. Batani, N. Piovella, R.B. Stephens, and F.N. Beg, "Improved laser-to-proton conversion efficiency in isolated reduced mass targets," *Appl. Phys. Lett.* **103**, 054102 (2013).
- P.A. Ni, S.M. Lund, C. McGuffey, N. Alexander, B. Aurand, J.J. Barnard, F.N. Beg, C. Bellei, F.M. Bieniosek, C. Brabetz, R.H. Cohen, J. Kim, P. Neumayer, M. Roth, and B.G. Logan, "Initial experimental evidence of self-collimation of target-normal-sheath-accelerated proton beam in a stack of conducting foils," *Phys. Plasmas* **20**, 083111 (2013).

7.4. Thesis

- Teresa Bartal, University of California San Diego, 2011.

P.O. BOX 85608 SAN DIEGO, CA 92186-5608 (858) 455-3000